Acta Crystallographica Section D
Biological Crystallography
ISSN 0907-4449

The structure of T_6 human insulin at 1.0 Å resolution

G. David Smith,[a,b]* Walter A. Pangborn[b,c] and Robert H. Blessing[b,c]

[a]Structural Biology and Biochemistry, Hospital for Sick Children, 555 University Avenue, Toronto, Ontario M5G 1X8, Canada, [b]Hauptman–Woodward Medical Research Institute, 73 High Street, Buffalo, NY 14203, USA, and [c]Department of Structural Biology, School of Medicine and Biomedical Sciences, State University of New York at Buffalo, Buffalo, NY, USA

Correspondence e-mail: gdsmith@sauron.psf.sickkids.on.ca

Received 7 October 2002
Accepted 23 December 2002

PDB Reference: T_6 human insulin, 1mso, r1msosf.

The structure of T_6 human insulin has been determined at 120 K at a resolution of 1.0 Å and refined to a residual of 0.183. As a result of cryofreezing, the first four residues of the B chain in one of the two crystallographically independent AB monomers in the hexameric $[Zn_{1/3}(AB)_2Zn_{1/3}]_3$ complex undergo a conformational shift that displaces the C^{α} atom of PheB1 by 7.86 Å relative to the room-temperature structure. A least-squares superposition of all backbone atoms of the room-temperature and low-temperature structures yielded a mean displacement of 0.422 Å. Omitting the first four residues of the B chain reduced the mean displacement to 0.272 Å. At 120 K, nine residues were found to exhibit two discrete side-chain conformations, but only two of these residues are in common with the seven residues found to have disordered side chains in the room-temperature structure. As a result of freezing, the disorder observed at room temperature in both ArgB22 side chains is eliminated. The close contact between pairs of $O^{\varepsilon 2}$ atoms in GluB13 observed at room temperature is maintained at cryotemperature and suggests that a carboxylate–carboxylic acid centered hydrogen bond exists [$-C(=O)-O\cdots H\cdots O-C(=O)-$] such that the H atom is equally shared between the two partially charged O atoms.

1. Introduction

Insulin is a polypeptide hormone that is critical for the metabolism of glucose. The insulin monomer consists of two chains, a 21-residue A chain and a 30-residue B chain, linked by a pair of disulfide bonds, A7–B7 and A20–B19; an additional intrachain disulfide bond links A6 and A11. While insulin is synthesized and stored in the pancreas as a hexamer, the hormonally active form is the monomer. The structure of the 2Zn insulin hexamer was first reported by Adams *et al.* (1969) and a comprehensive description of the room-temperature structure at 1.5 Å resolution and its biological implications were published by Baker *et al.* (1988). The structural results permitted not only a description of the fold of the insulin monomer and the organization of the hexamer, but also the identification of those invariant residues that lie on the surface of the monomer and most likely interact with the insulin receptor. The asymmetric crystal chemical unit consists of two insulin monomers related by a local twofold axis; the crystallographic threefold axis generates the insulin hexamer from the dimer. Two zinc ions, on opposite sides of the hexamer, are situated on the crystallographic threefold axis and each is octahedrally coordinated by three crystallographically related HisB10 $N^{\varepsilon 2}$ atoms and three water molecules.

The structure of T_6 porcine insulin has also been refined using the 1.5 Å room-temperature X-ray data in conjunction with 2.2 Å neutron data from a second crystal that had been deuterated by slow exchange of mother liquor with 70% D_2O (Wlodawer *et al.*, 1989). The two structures are nearly identical as evidenced by an r.m.s. deviation of 0.36 Å for the non-H protein atoms.

The results from numerous X-ray crystallographic (Baker *et al.*, 1988; Ciszak & Smith, 1994; Derewenda *et al.*, 1989) and spectroscopic studies (Kaarsholm *et al.*, 1989; Bloom *et al.*, 1995) have shown hexameric insulin to be an allosteric complex. In the presence of ions such as chloride or thiocyanate (Ciszak & Smith, 1994; Whittingham *et al.*, 1995), the first eight residues of three B chains in the hexamer undergo a conformational change from extended to α-helical. In order to avoid confusion in naming insulin hexamers, the component monomers are denoted T or R according to whether the first eight residues of the B chain have an extended (T) or an α-helical (R) conformation (Kaarsholm *et al.*, 1989). Thus, the hexamer formerly known as 2Zn insulin is now referred to as T_6, while the form produced in the presence of thiocyanate or chloride ion is called $T_3R_3^f$. In the presence of phenolic derivatives such as phenol (Derewenda *et al.*, 1989; Whittingham *et al.*, 1995), *m*-cresol or resorcinol (Smith *et al.*, 2000), the T$\rightarrow$R transition is driven to completion to produce an R_6 hexamer.

The results of crystallographic studies on R_6 insulin hexamers (Derewenda *et al.*, 1989; Smith *et al.*, 2000) have shown that room-temperature structures exhibit no major structural differences from those at 100 K. In contrast, $T_3R_3^f$ hexamers at 100 K exhibit an evidently pressure-induced phase change that produces a doubling of the *c* axis and two new zinc-binding sites between independent hexamers (Smith *et al.*, 2001; Von Dreele *et al.*, 2000). Reported here is the 1.0 Å resolution structure of T_6 human insulin at 120 K, which shows that the N-terminus of one B chain undergoes a conformational shift that moves the PheB1 C^α atom approximately 8 Å from its position in the room-temperature structure. There is little side-chain conformational disorder in either the room-temperature or cryotemperature structure, but some of the disorder occurs at different side chains in the two structures.

2. Experimental

2.1. Crystallization

Crystals of T_6 human insulin were grown in batch mode in microgravity aboard the US NASA Space Shuttle flight STS-86 using the UAB PCF (University of Alabama at Birmingham Protein Crystallization Facility) apparatus. Biosynthetic human insulin complexed with zinc was supplied by Lilly Research Laboratories. Buffers, salts and other reagents were purchased and used without further purification. The crystallizing media consisted of 5 mg ml^{-1} insulin, 0.01 *M* HCl, 0.007 *M* zinc acetate, 0.05 *M* sodium citrate and 17% acetone pH 6.3. The crystals were large, well shaped and free of inclusions.

Table 1
Primary crystal data *versus* temperature for T_6 insulin.

	T (K)	Space group	*a* (Å)	*c* (Å)	d_{min} (Å)	η† (°)	$\langle u^2\rangle^{1/2}$ ‡ (Å)	$\langle B_{iso}\rangle$ (Å^2)
Porcine	295	*R*3	82.5	34.0	1.50	—	0.526	21.8 (2)
Human	295	*R*3	82.91	34.13	1.50	0.27	0.493	19.2 (2)
	~150	*R*3	81.20	33.75	1.35	0.69	0.373	11.0 (2)
	120	*R*3	81.29	33.71	1.00	—	0.307	7.42 (6)

† The mosaic spread values η are Bragg peak full-widths at half-height for the HWI imaging-plate data as obtained from the *DENZO* (Otwinowski & Minor, 1997) data-processing program. ‡ The unit-cell-average isotropic equivalent root-mean-square atomic displacements $\langle u^2\rangle^{1/2} = (B_{iso}/8\pi^2)^{1/2}$ are from bulk-solvent and overall anisotropy corrected Wilson-scaling analyses (Blessing *et al.*, 1995).

2.2. Data measurement

The X-ray diffraction analyses of the crystals were performed in our laboratory at the Hauptman–Woodward Institute (HWI) and in the laboratory of Professors B.-C. Wang and John Rose at the University of Georgia (UGA). For the UGA experiments, we also had cooperation from Drs James Phillips and Steve Foundling of Bruker AXS, who demonstrated use of the Bruker SMART 2000 charge-coupled device (CCD) detector at UGA and the Bruker *SAINT* CCD data-reduction program.

At both HWI and UGA the X-ray sources were Rigaku 5 kW Cu rotating-anode generators fitted with a pyrolytic graphite crystal monochromator, a Molecular Structures Corp. liquid-nitrogen-vapor cryogas-stream cryotemperature device and a Rigaku R-AXIS IIc image-plate detector at HWI, and with a Siemens multi-layer Göbel diffraction-mirrors monochromator, a Molecular Structures Corporation X-Stream cryotemperature device and the Bruker CCD detector at UGA.

Preliminary room-temperature diffraction measurements were made on capillary-enclosed specimens and measurements at cryotemperatures were made on flash-frozen cryoprotected loop-mounted specimens. Cryoprotection was achieved by momentarily immersing the specimen crystals in solutions of, successively, x = 5, 10, 20 and 30% glycerol plus $(100 - x)\%(v/v)$ mother liquor and finally in a solution of 15% PEG 300, 25% glycerol and 60%$(v/v/v)$ mother liquor. These were, to our knowledge, the first cryofreezing experiments on T_6 insulin crystals and primary crystal data obtained at several temperatures are summarized in Table 1, which for comparison also includes room-temperature data (Baker *et al.*, 1988) for T_6 (or 2Zn) porcine insulin [ThrB30(human)$\rightarrow$Ala(porcine)].

The diffraction data used for the structure analysis were those measured at T = 120 K to d_{min} = 1.0 Å resolution in the UGA laboratory. The elapsed time between crystal growth on STS-86 and the measurement of data was a month. The data were recorded as ω-oscillation frames of $\Delta\omega = 0.25^\circ$ at $2\theta = 76$, φ = 30 and 150°, and then $\Delta\omega = 0.20^\circ$ at 2θ = 20, $\varphi = 120^\circ$. Because of time limitations on the instrument, a redundancy of only 1.8 was attained. The frames data were integrated and internally scaled using the *SAINT* program. The resulting reflections data were merged and averaged, with robust

Table 2
Data-reduction statistics for T_6 human insulin at 120 K to 1.00 Å resolution.

Resolution range (Å)	N_{meas}	N_{unique}	$\langle n_h \rangle$	Completeness (%)	R_{merge}† (%)	$\langle \lvert F_{\mathbf{h}} \rvert^2 / \sigma(\lvert F_{\mathbf{h}} \rvert^2) \rangle$
$30.4 \geq d \geq 1.00$	72631	41170	1.8	91.7	4.91	11.0
$30.4 \geq d \geq 4.00$		615	2.1	94.0	2.98	39.0
$1.02 \geq d \geq 1.00$		1688	1.4	75.0	36.9	2.3

† R_{merge} is the sample-size-corrected normalized mean absolute deviation, $R_{merge} = \sum_h [n_{\mathbf{h}}/(n_{\mathbf{h}}-1)]^{1/2} \sum_{i=1}^{n_{\mathbf{h}}} \lvert \lvert F_{\mathbf{h}} \rvert_i^2 - \langle \lvert F_{\mathbf{h}} \rvert^2 \rangle \rvert / \sum_{\mathbf{h}} \sum_{i=1}^{n_{\mathbf{h}}} \lvert \lvert F_{\mathbf{h}} \rvert_i^2 \rvert$.

resistant outlier down-weighting, using the program *SORTAV*, post-processed to improve weak data using the program *BAYES* and Wilson-scaled using the program *LEVY* (Blessing, 1997, 1999; Blessing *et al.*, 1998; French & Wilson, 1978). Data-reduction statistics are summarized in Table 2.

Highly redundant data were later measured to a resolution of 0.9 Å on two STS-86 crystals at the NSLS synchrotron at Brookhaven National Laboratories approximately six months after the crystals were obtained. Subsequent crystallization experiments of T_6 human insulin were performed in microgravity aboard Space Shuttle flight STS-95 and synchrotron data were measured on these crystals at Argonne National Laboratories. Although a considerable length of time had elapsed between crystal growth and data measurement, these crystals also diffracted to a resolution of 0.9 Å and highly redundant data were measured. For all of the synchroton data sets, R_{merge} in the higher resolution shells was unacceptably large, as were the residuals following refinement of the structure. Thus, the sets of synchrotron data were deemed to be inferior to those measured at UGA. The age of the crystals may in part account for the poor data quality and it is possible that even at 100 K the data in the highest resolution shells suffered from radiation damage.

2.3. Refinement

The initial model consisted of PDB entry 4ins (Baker *et al.*, 1988) from which all water molecules, zinc ions and alternate side chains were omitted. Each atom was assigned the unit-cell-average temperature factor obtained from the Wilson analysis in the program *LEVY*. 10% of the data were reserved for cross-validation and were never used during refinement (Brünger, 1992). A round of rigid-body refinement using *CNS* (Brünger, 1992; Pannu & Read, 1996; Adams *et al.*, 1997) and data from 15 to 4 Å resolution, treating the entire dimer as a rigid body, produced a residual of 0.30. A further round of refinement treating each monomer as a rigid body and using all data to 2.0 Å resolution yielded a residual of 0.32. The most prominent features of the $2F_o - F_c$ and $F_o - F_c$ σ_A-weighted maps (Read, 1990; Brünger *et al.*, 1997) were the two zinc ions.

The refinement was continued using maximum-likelihood torsion-angle dynamics, conjugate-gradient refinement or individual temperature-factor refinement in conjunction with an overall anisotropic temperature-factor correction and a bulk-solvent correction (Rice & Brünger, 1994; Brünger *et al.*, 1998; Adams *et al.*, 1997; Pannu & Read, 1996). Bonds to the two zinc ions were not restrained. The σ_A-weighted $2F_o - F_c$ and $F_o - F_c$ maps were carefully examined following each round of *CNS* refinement using *CHAIN* (Sack, 1988) or *XtalView* (McRee, 1999) and water molecules and alternate conformations of side chains were added in accord with good electron density. During the course of the refinement, H atoms were added at their theoretical positions and refined. The refinement of atomic thermal parameters in *CNS* can only be performed isotropically and the inability to perform an anisotropic refinement is most likely to be the primary reason that R and R_{free} could not be reduced to lower values. The final model consisted of 875 non-H protein atoms (1712 including H atom), two zinc ions, 165 water molecules with occupancies of unity and 61 water molecules with occupancies less than unity. An assessment of the quality of the Ramachandran plot by *PROCHECK* (Laskowski *et al.*, 1993) showed that the φ/ψ torsion angles for 81 of 86 residues lie in the most favored regions. Although the torsion angles for three residues (ThrB27.1,[1] ThrB27.2 and CysA7.2) lie in the additional allowed region, their positions are immediately adjacent to the most favored regions. Deviations of the SerA9.1 and SerA9.2 torsion angles from the most favored regions into the additional allowed region, a feature seen in all T-state monomers, are a result of strains imposed by the intrachain CysA6–CysA11 loop. The side chains of GlnA5.2, LeuA16.2, GlnB4.1, ValB12.1, LeuB17.1, ValB12.2, ValB18.2, GluB21.2 and ThrB27.2 were found to exist in two discrete orientations and were modeled and refined as such. The side chain of GluB21.2 was also modeled in two orientations, but the quality of the density would suggest that additional conformations are present with low occupancies. The side chains of GlnA15.2 and LysB29.2 were assigned occupancies of 0.5 owing to weak

Table 3
Data-refinement statistics.

No. of reflections	41242
Resolution range (Å)	30.4–1.0
R value	0.183
R_{free} value	0.201
Highest resolution shell	
Resolution range (Å)	1.06–1.00
No. of reflections	5238
Completeness (%)	77.6
R value	0.382
R_{free} value	0.397
Cross-validated estimated error (Å)	0.16
R.m.s. deviations from ideal	
Bond lengths (Å)	0.011
Bond angles (°)	2.2
Dihedral angles (°)	20.8
Improper angles (°)	1.10
Isotropic thermal model restraints (Å^2)	
Main-chain bonds	1.93
Main-chain angles	2.39
Side-chain bonds	3.84
Side-chain angles	3.89

[1] The decimal portion, 0.1 or 0.2, in the residue numbers refers to the monomer numbers, 1 or 2, respectively.

electron density. No density was observable for the side chain of PheB1.2. Refinement statistics are presented in Table 3.

3. Discussion

3.1. Monomer and dimer conformations

The structure of the T_6 human insulin dimer is illustrated in Fig. 1. The conformation of each monomer is nearly identical to that reported earlier for the room-temperature structure (Baker *et al.*, 1988), namely each A chain contains two α-helical segments connected by a short extended section of chain, while the B-chain conformations consist of a central α-helical segment flanked by two extended sections of chain. In the case of monomer 2, the N-terminal segment is extended, but the first four residues have undergone a shift which displaces the C^{α} of PheB1.2 by 7.86 Å. A least-squares superposition (Smith, 1993) of the insulin dimer of PDB entry 4ins (Baker *et al.*, 1988) and 3ins (Wlodawer *et al.*, 1989) onto the dimer of the present study, minimizing the displacements of the A11–A19 and B11–B19 backbone atoms, produced a mean displacement for those atoms used in the optimization of 0.167 and 0.168 Å and a displacement for all backbone atoms of 0.422 and 0.427 Å for PDB entries 4ins and 3ins, respectively; if the first four residues of the B chain in monomer 2 are excluded from the calculation, the respective mean displacements for all the remaining backbone atoms are reduced to 0.272 and 0.277 Å, respectively. The C^{α} displacements between the present cryotemperature structure and the room-temperature structure (PDB entry 4ins) are illustrated in Fig. 2(*a*) for the A chains and in Fig. 2(*b*) for the B chains.

In the room-temperature structure, the conformations of the two monomers are nearly identical and a least-squares superposition of monomer 1 onto monomer 2, minimizing displacements of the residues listed above, resulted in a mean displacement of 0.220 Å for those backbone atoms used in the superposition fitting and of 0.753 Å for all backbone atoms. In the cryotemperature structure, the corresponding values are 0.293 and 1.279 Å, respectively. A histogram illustrating these displacements is shown in Fig. 3. Of particular note are the differences at the N- and C-termini of the B chains. The large displacement at the N-terminus is a result of the shift observed in monomer 2, while the displacement at the C-terminus is a result of a conformational difference that is also observed in the room-temperature structure.

3.2. Side-chain disorder and conformational differences

Seven and nine side chains are observed to occupy two discrete conformations in the room-temperature and cryo-

Figure 1
Structure of the T_6 human insulin dimer as illustrated by *SETOR* (Evans, 1993). A chains are colored red, B chains green, HisB10 side chains cyan, disulfide bonds yellow and zinc ions blue. Monomer 1 is at the top left, while monomer 2 is at the bottom right.

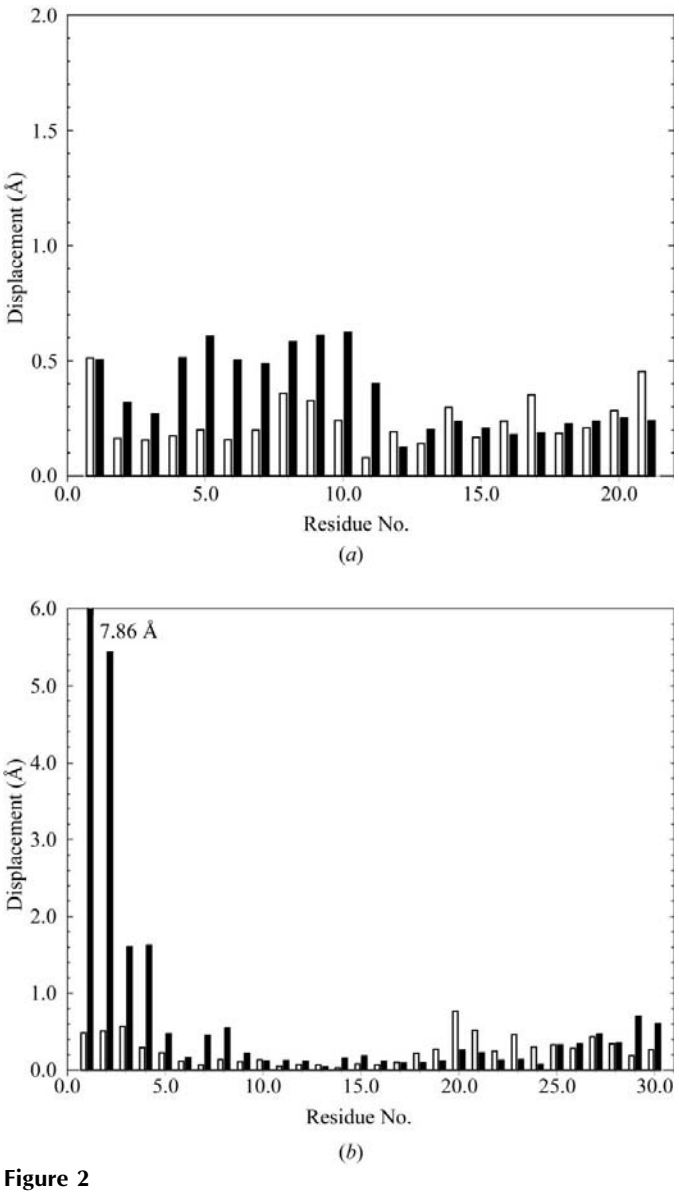

Figure 2
Histogram illustrating the C^{α} displacements of (*a*) the A chains and (*b*) the B chains following the superposition of the dimer onto that of PDB entry 4ins. White bars refer to monomer 1 and black bars to monomer 2.

temperature structures, respectively, although their identities are not the same in all cases. Observed as disordered in the room-temperature structure were GlnB4.1, ValB12.1, GluB21.1, ArgB22.1, ThrB27.1, ArgB22.2 and LysB29.2. At 120 K, disorder was observed at GluB4.1, ValB12.1, GluB17.1, GlnA5.2, LeuA16.2, ValB12.2, ValB18.2, GluB21.2 and ThrB27.2. Only two residues are found to be in common to the above lists, GlnB4.1 and ValB12.1.

While the disorder in ValB12.1 is nearly identical in the two structures, significant differences exist between the disordered side chains in GlnB4.1. ValB12 is located on the surface of the monomer, but makes important hydrophobic contacts that help to stabilize the formation of the dimer. In the present study, the side chains of ValB12 in both monomers were found to occupy two discrete positions. In both monomers, $C^{\gamma 1}$ is found to be either nearly *trans* to the nitrogen or to the carbonyl carbon of ValB12. However, if $C^{\gamma 1}$ is *trans* to the nitrogen in the side chains of both residues at the same time, a steric clash occurs, as the distance between the two $C^{\gamma 1}$ atoms is 2.25 Å. No other combinations of the observed conformations produce short contacts and therefore when one side chain of one ValB12 adopts the $C^{\gamma 1}$ *trans* to nitrogen conformation, the second ValB12 side chain must adopt an orientation *trans* to the carbonyl O atom.

Side chains which show significant differences in conformation in the two structures include GluA17.1, AsnA21.1, LysB29.1, GluB21.2 and LysB29.2.

3.3. PheB1.2 displacement

In the room-temperature structure, the PheB1 residues lie on the dimer–dimer interface adjacent to pairs of TyrA14 residues and between pairs of LeuA13 and GluA17 residues. The phenylalanine side chains lie just under the surface of the hexamer and the amino N and carbonyl O atoms lie on the surface. This arrangement is illustrated in Fig. 4. As a result of freezing, the first four residues of the B chain in monomer 2 are displaced up to 7.86 Å away from the dimer–dimer interface and towards the exterior of the hexamer, placing the side chain of ValB2.2 on the surface of the hexamer. No electron density was observed for the side chain of PheB1.2, but based upon the position of the C^{β} atom, the disordered phenyl group probably lies just under the surface of the hexamer.

The amino N atom of ValB2.2 forms a hydrogen bond (2.84 Å) to $O^{\varepsilon 2}$ of a symmetry-related GluB21.1 residue. While the side chain of GluA17.1, which is adjacent to PheB1.2, undergoes a change of conformation, the carboxyl group maintains the same relative orientation at 120 K as at room temperature. Owing to the displacement of PheB1.2, GluA17.1 is displaced towards the hexamer surface and this moves the C^{δ} atom 0.90 Å. In contrast, the side chains of GluA17.2 of the room-temperature and 120 K structures are nearly superimposable and the displacement between the two C^{δ} atoms is only 0.45 Å. The displacement of the four N-terminal residues does not produce any additional movement of protein atoms, but does require a rearrangement of the water structure at the surface of the hexamer as well as the addition of water molecules to occupy the vacated space.

3.4. Zinc ion coordination

As was the case in the room-temperature structure, each zinc ion is octahedrally coordinated by $N^{\varepsilon 2}$ of three symmetry-related HisB10 side chains (at 2.09 and 2.10 Å for trimer 1 and trimer 2, respectively); the coordination sphere of each zinc ion is completed by three symmetry-related water molecules (at 2.20 and 2.23 Å for trimer 1 and trimer 2, respectively). In the case of trimer 2, an additional three water molecules reside

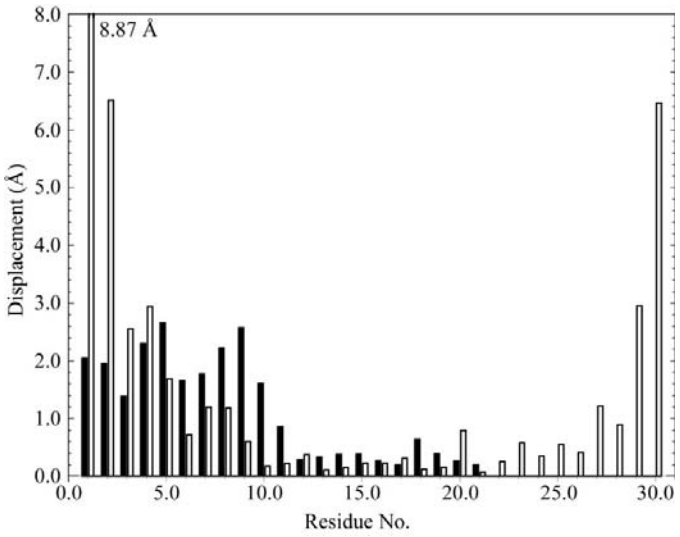

Figure 3
Histogram illustrating the C^{α} displacements following a superposition of backbone atoms of monomer 1 onto monomer 2. Black bars represent A chains and white bars B chains.

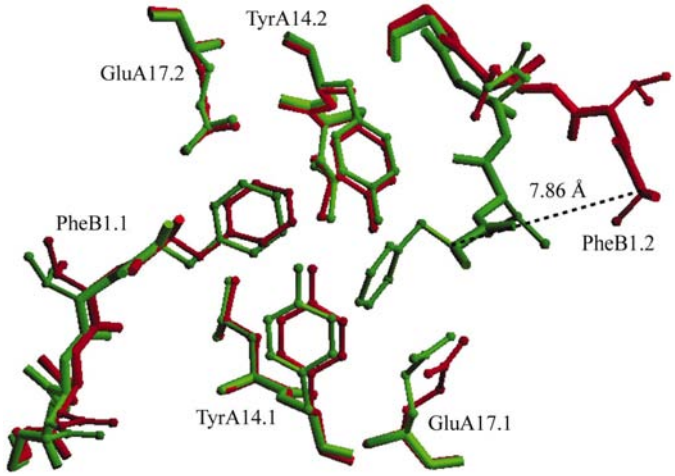

Figure 4
SETOR drawing (Evans, 1993) showing the vicinity of the PheB1 residues, viewed towards the center of the hexamer. The room-temperature structure is colored green, while the 120 K structure is colored red. Residues labeled *X*.1 are related to the primary monomer by the threefold crystallographic symmetry element $(-x + y, -x, z)$. The dotted line shows the displacement of the C^{α} of PheB1.2 by 7.86 Å relative to the T_6 porcine room-temperature structure.

above the three zinc-coordinating waters with water–water contacts of 2.35 Å and the electron density is unambiguous. However, for trimer 1 there is continuous electron density above the zinc ion and its coordinating waters. This density has been modeled as disordered water molecules, but it is possible that a disordered anion such as citrate may in fact occupy this site.

3.5. GluB13 residues and the water structure in the hexamer core

Unlike the T_3R_3 or R_6 hexamers, in which the side chains of GluB13 are observed to occupy discrete alternate conformations (Smith *et al.*, 2000, 2001), the electron density shown in Fig. 5 is unambiguous in showing that each of the independent GluB13 side chains adopts a single and nearly identical conformation ($\chi^1 = -70.4^\circ$, $\chi^2 = -77.6^\circ$, $\chi^3 = -17.6^\circ$ in monomer 1; $\chi^1 = -75.1^\circ$, $\chi^2 = -81.8^\circ$, $\chi^3 = -15.2^\circ$ in monomer 2), with the planes of the carboxylate groups nearly parallel to the crystallographic threefold axis. A very short contact, 2.46 Å, exists between the two independent GluB13 $O^{\varepsilon 2}$ atoms.

A well ordered three-layer water cluster, each layer being perpendicular to the crystallographic threefold axis and illustrated in Fig. 6, lies within the central portion of the hexamer. There are no direct hydrogen-bonded contacts between the layers, which are separated by approximately 3.2 Å. Layer 1 contains a total of 13 symmetry-related waters (634, 624, 630 in the central portion of the hexamer; 625 and 629 at the dimer–dimer interface) that lie between the HisB10.1 side chains and the GluB13 cluster. Layer 2 contains three symmetry-related waters, 706, which are central and adjacent to the GluB13 side chains. Layer 3, also containing 13 water molecules and related to layer 1 by the non-crystallographic twofold axis, lies between HisB10.2 and the GluB13 cluster. This layer contains waters 606, 621 and 645 in the central core, with waters 649 and 680 lying on the dimer–dimer interface. Only layer 2 is constrained to be planar, but layers 1 and 3 have mean deviations from planarity of 0.00 and 0.01 Å, respectively. An additional water molecule, 741, lies between layers 2 and 3 and forms hydrogen-bonded contacts to the GluB13 carboxylate groups.

An examination of a Connolly surface (Connolly, 1983) constructed around the central core protein atoms in conjunction with a water van der Waals surface shows that the water molecules are closely packed within the site and that there is little room for any additional solvent. All hydrogen-bonded contacts involving these water molecules are listed in Table 4. Through this extensive hydrogen-bonding network, water molecules form hydrogen bonds from the carboxylate O atoms of GluB13 in one monomer to O^{γ} of SerB9, $N^{\delta 1}$ of HisB10 and O of HisB10 in the second monomer.

The mean B_{iso} for all of the waters within the central core is 19.6 $Å^2$ compared with a mean B_{iso} of 23.9 $Å^2$ and 10.8 $Å^2$ for all water molecules and all protein atoms, respectively. The mean separation between the waters within the cluster and

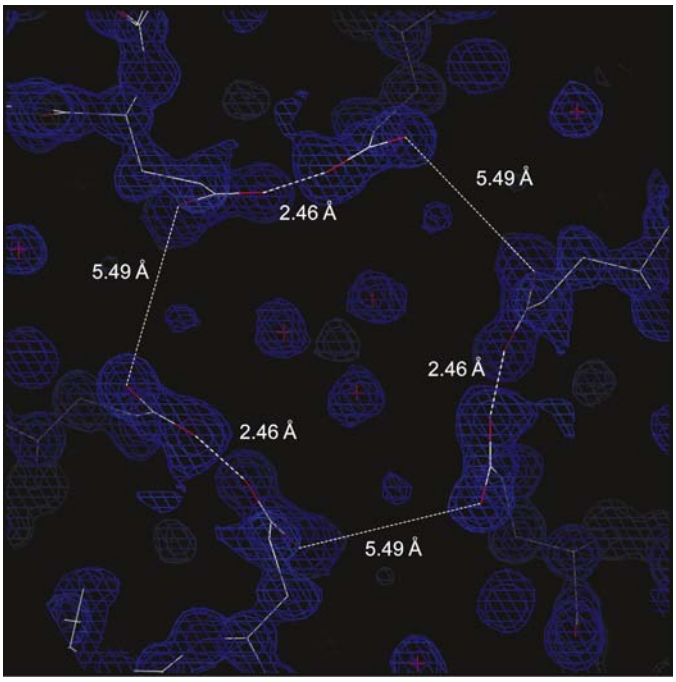

Figure 5
View down the crystallographic threefold axis illustrating the GluB13 cluster in the center of the T_6 human insulin hexamer. Contacts between adjacent carboxyl O atoms are illustrated as dotted lines. The σ_A-weighted $2F_o - F_c$ maps have been contoured at 1σ.

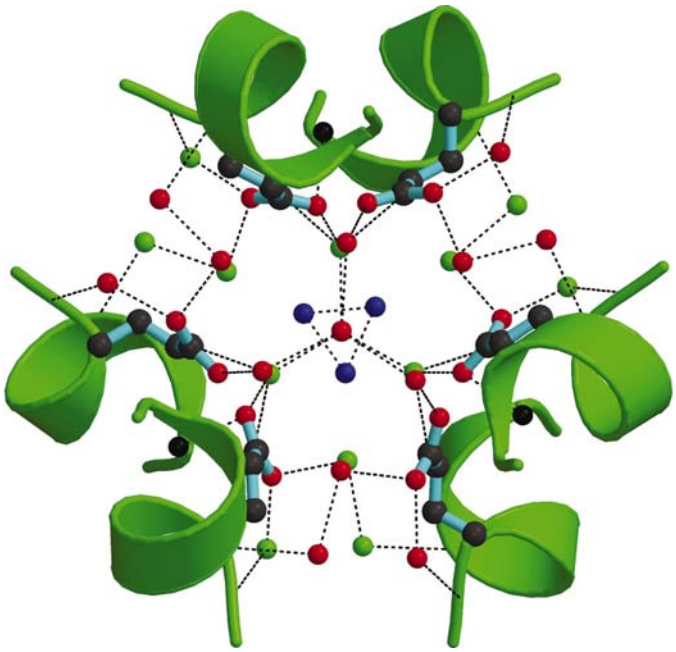

Figure 6
The central core of the hexamer illustrating the three layers of water that interact with the GluB13 side chains as viewed down the crystallographic threefold axis. Water molecules in layer 1 are colored red, layer 2 blue and layer 3 green. Water 634 of layer 1 (red) lies on the crystallographic threefold axis and obscures water 606 which also lies on the threefold axis. Hydrogen-bonded contacts are illustrated as black dotted lines. For the sake of clarity, main-chain peptide O atoms have been omitted as well as atoms and contacts involving HisB10. Water 741, which lies between layers 2 and 3, is colored black. This figure was prepared with the programs *MOLSCRIPT* (Kraulis, 1991) and *RASTER3D* (Merritt & Murphy, 1994).

Table 4
Hydrogen-bonded contacts involving water within the three layers in the central core of the hexamer.

Waters 606 and 634 lie on the crystallographic threefold axis. To avoid confusion, all three contacts related by the threefold axis in layer 2 are listed. Symmetry-related contacts for layers 1 and 3 are not listed.

Atoms		Distance (Å)	Symmetry
Layer 1			
634 O	624 O	2.91	x, y, z
624 O	GluB13.2 $O^{\varepsilon 2}$	2.80	x, y, z
624 O	SerB9.1 O^{γ}	2.59	x, y, z
630 O	625 O	2.88	x, y, z
630 O	HisB10.1 $N^{\delta 1}$	2.89	x, y, z
630 O	GluB13.2 $O^{\varepsilon 1}$	2.98	x, y, z
625 O	HisB10.1 O	2.78	x, y, z
639 O	GluB13.2 O	2.72	x, y, z
639 O	GluB13.2 $O^{\varepsilon 1}$	2.71	x, y, z
Layer 2			
706 O	706 O	2.37	x, y, z
706 O	706 O	2.37	$-y, x - y, z$
706 O	706 O	2.37	$-x + y, -x, z$
Layer 3			
606 O	621 O	2.74	x, y, z
621 O	GluB13.1 $O^{\varepsilon 2}$	2.71	x, y, z
621 O	SerB9.2 O^{γ}	2.75	x, y, z
645 O	649 O	2.94	$-x + y, -x, z$
645 O	HisB10.2 $N^{\delta 1}$	2.83	x, y, z
645 O	GluB13.1 $O^{\varepsilon 1}$	2.98	$-x + y, -x, z$
649 O	HisB10.2 O	2.80	x, y, z
680 O	GluB13.1 O	2.78	x, y, z
680 O	GluB13.1 $O^{\varepsilon 1}$	2.62	x, y, z
741 O	GluB13.1 $O^{\varepsilon 2}$	2.49	x, y, z
741 O	GluB13.1. $O^{\varepsilon 1}$	3.20	x, y, z

their non-crystallographic dyad-related equivalent positions is 0.46 Å, while the mean separations between waters in the central core of the present study and PDB entries 4ins and 3ins are 0.55 and 0.68 Å, respectively.

In PDB entry 4ins, a short contact of 2.59 Å was observed between pairs of independent GluB13 $O^{\varepsilon 2}$ atoms (Baker *et al.*, 1988) and the authors concluded that as the carboxylate groups should be completely ionized, the short contact was most likely to be a result of the large standard deviations of the side-chain atomic positions. In the joint X-ray/neutron refinement (Wlodawer *et al.*, 1989), the distance between the $O^{\varepsilon 2}$ atoms was 2.37 Å. The neutron-density map in this region was 'not very clear' and no density corresponding to a D atom was seen. Since the authors were unable to confirm the presence of a hydrogen bond (pH 6.5), they concluded that this was a non-bonded interaction instead.

In the present study, the $O^{\varepsilon 2}\cdots O^{\varepsilon 2}$ contact is 2.46 Å as noted above, but the absence of electron density corresponding to a H atom in either the $2F_o - F_c$ density or $(F_o - F_c)$ difference maps is not surprising with a residual of 0.183.

Since the protein was crystallized at a pH of 6.3, one would normally expect the carboxyl groups to be ionized. If this were the case, however, the central core of the hexamer would contain a net charge of −6 and would also contain three very short contacts between partially charged O atoms, a very unlikely situation.

Titration experiments performed by Kaarsholm *et al.* (1990) caused these authors to conclude that one carboxylate, GluB13, is masked with an isoionic point of 6.4. At a crystallization pH of 6.3, approximately half or three of the six GluB13 side chains would be protonated and available to donate a proton to a hydrogen-bond acceptor. In both the room-temperature and 120 K structures, three short ∼2.5 Å contacts exist between the $O^{\varepsilon 2}$ atoms of the two independent GluB13 side chains, and the GluB13 carboxylate O atoms accept hydrogen bonds from water molecules (Fig. 6). Based on both the titration and structural results, we would suggest that a carboxylate–carboxylic acid centered hydrogen bond exists between the two GluB13 $O^{\varepsilon 2}$ atoms [—C(═O)—O···H···O—C(═O)—] such that the H atom is shared more or less equally between the two partially charged O atoms.

Table 5
Contacts (Å) involving the first four residues of each *B* chain.

Atoms		120 K	Room temperature	Symmetry
PheB1.1 N	GluA17.2 $O^{\varepsilon 2}$	2.75	2.78	$-y, x - y, z$
PheB1.2 N	GluA17.1 $O^{\varepsilon 2}$	9.53	2.96	$y–x, –x, z$
ValB2.2 N	GluB21.1 $O^{\varepsilon 2}$	2.84	6.97	$y -x, -x, z$
AsnB3.2 O	SerA9.1 O^{γ}	2.74	5.35	$y -x, -x, z - 1$
GlnB4.1 O	CysA11.1 N	3.02	2.99	x, y, z
GlnB4.1 $O^{\varepsilon 1}$	LeuB17.2 O	2.83	3.18	$-y, x - y, z$
GlnB4.2 O	CysA11.2 N	4.15	3.16	x, y, z
GlnB4.1 N	CysA11.1 O	2.82	2.71	x, y, z
GlnB4.2 N	CysA11.2 O	5.08	3.13	x, y, z

3.6. Hydrogen-bonding differences

Given the near identity in the topology of the two structures, it is not surprising that there are few differences in the main-chain hydrogen-bonding patterns within the α-helices and β-sheets. Many of the differences are most likely to result from errors in coordinate positions or from the omission of an alternate side-chain conformation. Within the intra-A-chain hydrogen-bonded contacts, a contact of 2.98 Å exists between the $N^{\varepsilon 2}$ atom of GlnA5.1 and $O^{\varepsilon 1}$ of GlnA15.1 in the 120 K structure, but at room temperature the distance is 3.50 Å. This difference results from a small change in conformation of the GlnA15.1 side chain, as the difference between the C^{δ} atoms is calculated to be nearly 0.5 Å.

Differences in the intra-B-chain hydrogen bonds are particularly noteworthy for contacts between CysB19 and ArgB22. At 120 K, the distance between CysB19.1 O and ArgB22.1 N^{ε} is 3.15 Å, but at room temperature the distance has increased to 3.65 Å. This difference primarily arises from slight displacements in main-chain conformations and an examination of Fig. 2(*b*) shows a C^{α} displacement of 0.77 Å for GlyB20.1. In monomer 2, a contact of 3.18 Å is noted between the carbonyl O of CysB19 and the N^{ε} atom of an alternate side-chain conformation, but in the 120 K structure the ArgB22.2 side chain is not disordered and is well removed from the CysB19 residue. Differences in hydrogen bonding at AsnA21.2 are also noted and are a result of small displacements of this residue relative to the room-temperature structure as shown in Fig. 2(*a*).

As a result of the displacement of the B-chain N-terminus of monomer 2, significant alterations in the interhexamer

hydrogen-bonding pattern occur and are listed in Table 5. For comparison purposes, contacts involving the first four residues of monomer 1 are also listed. Examination of this table shows that while one hydrogen bond in the room-temperature structure is disrupted, two additional bonds are formed as a result of the displacement of the N-terminus of the B chain. The intra-monomer hydrogen-bonding pattern involving main-chain atoms of GlnB4.2 are also disrupted, but in this case two hydrogen bonds are lost with no new ones being formed.

4. Conclusions

The results from this structure analysis and the comparison with the room-temperature structure again demonstrate that cryotemperatures can produce significant structural differences, as was also observed in the cryotemperature structure of $T_3R_3^f$ human insulin (Smith *et al.*, 2001 and references therein). Although there is a one amino-acid difference between porcine and human insulin [ThrB30(human)→Ala(porcine)], this is unlikely to have any effect upon the temperature-induced conformational change, as this B-chain C-terminal residue is well removed from either of the B-chain N-termini. While frozen crystals are typically required at a synchrotron source, efforts should be made to provide some structural information, such as a lower resolution structure at room temperature, in order to verify that no large conformational changes or phase changes occur as a result of freezing. Based upon the two T_6 insulin structures and their differences, it is not obvious why the N-terminus of monomer 2 is displaced, nor is it clear why cryotemperatures affect only monomer 2 and not monomer 1. While there is a net loss of one hydrogen bond in the affected region compared with the room temperature structure, additional gains in energy must be produced in the vicinity to compensate for the loss of hydrogen-bonding energy.

This study also shows that some residues are statistically disordered, regardless of the temperature (ValB12.1). However, in the case of the ArgB22 residues, cryofreezing eliminates the disorder. It seems likely that some of the residues that are observed to be disordered in the present study may also have been disordered at room temperature (ValB12.2, ValB18.2, LeuA16.2); the disorder was resolved in the present study as a result of the higher resolution data in conjunction with cryotemperatures.

The close contacts between the side chains of the GluB13 residues have been an unresolved issue, although given the biochemical evidence and the reproducible structural results, a hydrogen bond must be present. Our results suggest that this is a centered hydrogen bond, but the resolution of this issue will require either a charge-density or a neutron-diffraction study. The fact that disorder and significant changes in conformation of the GluB13 residues are observed in R-state trimers ($T_3R_3^f$ or R_6) seems to suggest that the constellation of GluB13 side chains in the center of the hexamer play a role in the T→R transition. Results from studies in progress to experimentally map electronic charge density and electrostatic potential distributions will provide additional information regarding the T→R transition as well as the protonation state of the GluB13 side chains.

The authors wish to thank Dr Marianna Long and Ms Vickie King of the PCF at the University of Alabama, Birmingham for setting up the microgravity crystal-growth experiments, Lilly Research Laboratories for a generous gift of biosynthetic human insulin, Drs B.-C. Wang and John Rose for the use of their diffraction facilities, and Drs James Phillips and Steve Foundling for assistance in data measurement and processing. The microgravity crystallization experiments were supported by NASA grant NCC8-126 to Dr Lawrence J. DeLucas. This research was supported by NIH grant GM56829 (RHB).

References

Adams, M. J., Blundell, T. L., Dodson, E. J., Dodson, G. G., Vijayan, M., Baker, E. N., Harding, M. M., Hodgkin, D. C., Rimmer, B. & Sheat, S. (1969). *Nature (London)*, **224**, 491–495.
Adams, P. D., Pannu, N. S., Read, R. J. & Brünger, A. T. (1997). *Proc. Natl Acad. Sci. USA*, **94**, 5018–5023.
Baker, E. N., Blundell, T. L., Cutfield, J. F., Cutfield, S. M., Dodson, E. J., Dodson, G. G., Hodgkin, D. C., Hubbard, R. E., Isaacs, N. W., Reynolds, C. D., Sakabe, K., Sakabe, N. & Vijayan, N. M. (1988). *Philos. Trans. R. Soc. London Ser. B*, **319**, 369–456.
Blessing, R. H. (1997). *J. Appl. Cryst.* **30**, 421–426.
Blessing, R. H. (1999). *Lecture Notes, Crystallographic Computing School on 'Frontiers in Computational Crystallography'*, Hinxton, Cambridge, England, August 1999.
Blessing, R. H., Guo, D. Y. & Langs, D. A. (1995). *Acta Cryst.* D**52**, 257–266.
Blessing, R. H., Guo, D. Y. & Langs, D. A. (1998). *Direct Methods for Solving Macromolecular Structures*, NATO ASI Series *C*: *Mathematical and Physical Sciences*, Vol. 507, edited by S. Fortier, pp. 47–71. Dordrecht: Kluwer Academic Publishers.
Bloom, C. R., Choi, W., Brzovic, P. S., Huang, J. J., Kaarsholm, N. C. & Dunn, M. F. (1995). *J. Mol. Biol.* **245**, 324–330.
Brünger, A. T. (1992). *Nature (London)*, **355**, 472–474.
Brünger, A. T., Adams, P. D., Clore, G. M., Delano, W. L., Gros, P., Grosse-Kunstleve, R. W., Jiang, J., Kuszewski, J., Nilges, M., Pannu, N. S., Read, R. J., Rice, L. M., Simonson, T. & Warren, G. L. (1998). *Acta Cryst.* D**54**, 905–921.
Brünger, A. T., Adams, P. D. & Rice, L. M. (1997). *Structure*, **5**, 325–336.
Ciszak, E. & Smith, G. D. (1994). *Biochemistry*, **33**, 1512–1517.
Connolly, M. L. (1983). *J. Appl. Cryst.* **16**, 548–558.
Derewenda, U., Derewenda, Z., Dodson, E. J., Dodson, G. G., Reynolds, C., Sparks, K., Smith, G. D. & Swenson, D. C. (1989). *Nature (London)*, **338**, 594–596.
Evans, S. V. (1993). *J. Mol. Graph.* **6**, 244–245.
French, S. & Wilson, K. (1978). *Acta Cryst.* A**34**, 517–525.
Kaarsholm, N. C., Havelund, S. & Hougaard, P. (1990). *Arch. Biochem. Biophys.* **283**, 496–502.
Kaarsholm, N. C., Ko, H. & Dunn, M. F. (1989). *Biochemistry*, **28**, 4427–4435.
Kraulis, P. (1991). *J. Appl. Cryst.* **24**, 946–950.
Laskowski, R. A., MacArthur, M. W., Moss, D. S. & Thornton, J. M. (1993). *J. Appl. Cryst.* **26**, 283–291.
McRee, C. E. (1999). *J. Struct. Biol.* **125**, 156–165.
Merritt, E. A. & Murphy, M. E. P. (1994). *Acta Cryst.* D**50**, 869–873.
Otwinowski, Z. & Minor, W. (1997). *Methods Enzymol.* **276**, 307–326.
Pannu, N. S. & Read, R. J. (1996). *Acta Cryst.* A**52**, 659–668.

Read, R. J. (1990). *Acta Cryst.* A**46**, 900–912.
Rice, L. M. & Brünger, A. T. (1994). *Proteins Struct. Funct. Genet.* **19**, 277–290.
Sack, J. S. (1988). *J. Mol. Graph.* **6**, 244–245.
Smith, G. D. (1993). *PROFIT. A Locally Written Program for Orienting One Protein Molecule onto Another by a Least-Squares Procedure.* Hauptman–Woodward Medical Institute, Buffalo, USA.
Smith, G. D., Ciszak, E., Magrum, L. A., Pangborn, W. A. & Blessing, R. H. (2000). *Acta Cryst.* D**56**, 1541–1548.
Smith, G. D., Pangborn, W. A. & Blessing, R. H. (2001). *Acta Cryst.* D**57**, 1091–1100.
Von Dreele, R. B., Stephens, P. W., Smith, G. D. & Blessing, R. H. (2000). *Acta Cryst.* D**56**, 1549–1553.
Whittingham, J. L., Chaudhurri, S., Dodson, E. J., Moody, P. C. E. & Dodson, G. G. (1995). *Biochemistry*, **34**, 15553–15563.
Wlodawer, A., Savage, H. & Dodson, G. (1989). *Acta Cryst.* B**45**, 99–107.